Tuning Cellulose Nanocrystal Gelation with Polysaccharides and Surfactants

ARTICLE *in* LANGMUIR · FEBRUARY 2014

Impact Factor: 4.46 · DOI: 10.1021/la404977t · Source: PubMed

4 AUTHORS, INCLUDING:

Zhen Hu
McMaster University
5 PUBLICATIONS **27** CITATIONS
SEE PROFILE

Emily Dawn Cranston
McMaster University
30 PUBLICATIONS **642** CITATIONS
SEE PROFILE

Langmuir

Article

pubs.acs.org/Langmuir

Tuning Cellulose Nanocrystal Gelation with Polysaccharides and Surfactants

Zhen Hu, Emily D. Cranston, Robin Ng, and Robert Pelton*

Department of Chemical Engineering, McMaster University, Hamilton, Canada L8S 4L71

Supporting Information

ABSTRACT: Gelation of cellulose nanocrystal (CNC) dispersions was measured as a function of the presence of four nonionic polysaccharides. Addition of hydroxyethyl cellulose (HEC), hydroxypropyl guar (HPG), or locust bean gum (LBG) to CNC dispersions induced the gelation of dilute CNC dispersions, whereas dextran (DEX) did not. These behaviors correlated with adsorption tendencies; HEC, HPG, and LBG adsorbed onto CNC-coated quartz crystal microbalance sensors, whereas DEX did not adsorb. We propose that the adsorbing polysaccharides greatly increased the effective volume fraction of dilute CNC dispersions, driving more of the nanocrystals into anisotropic domains. SDS and Triton X-100 addition disrupted HEC−CNC gels whereas CTAB did not. Surface plasmon resonance measurements with CNC-coated sensors showed that SDS and Triton X-100 partially removed adsorbed HEC, whereas CTAB did not. These behaviors illustrate the complexities associated with including CNC dispersions in formulated products: low CNC contents can induce spectacular changes in rheology; however, surfactants and soluble polymers may promote gel formation or induce CNC coagulation.

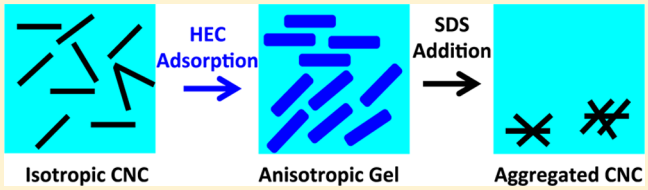

INTRODUCTION

Although cellulose nanocrystals (CNC) were first reported in 1949,[1] only now is CNC entering the marketplace in commercial scale quantities. Also called nanocrystalline cellulose or cellulose whiskers, CNC particles are stiff colloidal sized rods, approximately 100 × 10 × 10 nm³.[2,3] Aqueous CNC suspensions can be colloidally stable in water because of surface charged sulfate half-ester, carboxylate, or phosphate ester groups,[4] depending on the CNC preparation method. As a new, green, and sustainable material, CNC is currently being evaluated in a variety of applications, including as reinforcing materials in nanocomposites,[5] as stabilizers for emulsions and foams,[6] and as components of drilling fluids.[7] The recent patent literature is rich with descriptions of many other potential applications, many of which exploit the intrinsic thickening and gelation properties of small rod-shaped particles. However, most formulated chemical products, including food and cosmetics, are complex mixtures of surfactants and polymers in relatively high ionic strength solutions. Herein we set out initial results describing the influence of nonionic, water-soluble polymers on the rheological and gelation behaviors of CNC dispersions at high ionic strength. In addition, we show that surfactants alter the behavior of CNC−polymer mixtures. Our ultimate goal is to develop generic design rules for CNC-containing formulations. The following paragraphs summarize the relevant literature.

CNC Phase Behavior. Colloidal stability has a profound influence on CNC dispersion behavior. Colloidally unstable CNC particles adhere upon contact giving precipitates with dilute dispersions and a space filling gel floc for concentrated dispersions. Sulfated CNC particles are electrostatically stabilized by high surface charge densities of approximately 1 charge group for every 10 surface anhydroglucose units.[8] The critical coagulation concentration of NaCl for sulfated CNC[9−11] and for much longer nanofibrillated cellulose[12] is in the range 10−50 mM, whereas Araki[13] reported aggregation of carboxylated CNC between 100 and 500 mM NaCl.

Colloidally stable dispersions of rod-shaped particles undergo isotropic phase-to-isotropic phase + anisotropic phase transitions at low volume fractions, behaviors predicted by Onsager,[14] Flory,[15] and others.[16] Dong et al. published a detailed study of the phase compositions as functions of electrolyte concentration and counterion type.[17,18] Because they found that the major features of their experimental results were captured with SLO (Stroobants, Lekkerkerker, Odijk) theory,[16,19] we show some of the model's predictions in Figure 1 as plots of the volume fractions of the anisotropic (presumed to be nematic) phase, ϕ_a, as functions of the overall CNC concentration. The model parameters, including $1/\kappa$, the Debye length, and De, the effective diameter of the CNC rods, are shown in the Figure. The biphasic regions sits between two CNC concentrations; C_1 is the CNC concentration corresponding to the isotropic phase-to-isotropic phase + anisotropic phase transition, and C_2 is the total CNC concentration at which the isotropic phase disappears. For the middle curve in Figure 1, the biphasic (isotropic + anisotropic) region falls in the narrow CNC concentration range between C_1 = 36 g/L and C_2 = 47 g/L.

Received: December 30, 2013
Revised: February 16, 2014
Published: February 23, 2014

   dx.doi.org/10.1021/la404977t | Langmuir 2014, 30, 2684−2692

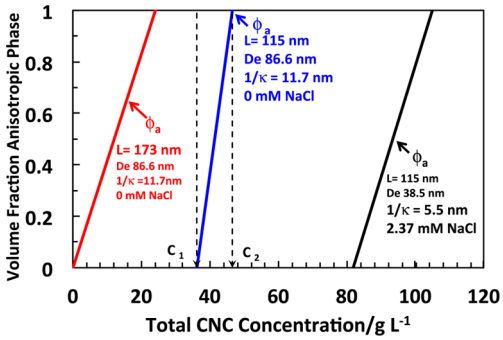

Figure 1. Schematic illustration of CNC phase behaviors modeled by SLO theory.[16,19] Parameters for the two L = 115 nm curves were taken directly from Table 2 of Dong et al.[17] L is the nanocrystals length, De is the nanocrystals effective width, and $1/\kappa$ is the Debye length.

Comparison of the three cases in Figure 1 illustrates two important variables controlling phase behavior. Salt addition lowered the effective diameter of the nanocrystals, De, shifting the biphasic region to higher concentrations and broadening the range of the biphasic region. By contrast, the SLO model predicts that lengthening the CNC particles by 50% shifts the biphasic region to a much lower CNC concentration, while increasing the width of the biphasic region.

We emphasize that the simulated phase behaviors in Figure 1 are approximate—Dong et al.[17,18] showed that CNC concentrations are not constant in the biphasic regions. Furthermore, Wierenga and Philipse[20] make the interesting point that rod suspensions are often present as unstable glasses if the rods have insufficient mobility to form the thermodynamically favored mixed phases.

CNC is a promising additive for aqueous formulations because low concentrations can give large increases in viscosities.[9,21−24] Our focus is on the interplay of water-soluble polymers and surfactants with CNC rheology and gel formation. The first publications describing CNC were from Gray's group and described interactions with water-soluble polymers dextran (DEX) and dye-labeled dextran.[25−27] Neither dextran nor the labeled dextran adsorbed onto the sulfated CNC surfaces. Furthermore, nonionic dextran did not influence the phase behavior of anisotropic suspensions (i.e., CNC concentrations > C_2). By contrast, dextran labeled with ionic dyes shifted C_2 to higher values, giving a coexisting isotropic phase. Some combinations of nonionic dextran and labeled ionic dextran gave two isotropic phases in equilibrium with the anisotropic phase.

Boluk[28] reported dynamic viscosity measurements of dilute CNC suspensions in hydroxyethyl cellulose (HEC) or carboxymethyl cellulose (CMC) solutions. HEC is a popular thickener for formulated chemical products because the polymer does not interact strongly with surfactants[29] and tends not to adsorb onto surfactant-coated surfaces.[30] They found that CNC greatly increased the viscosity of HEC solutions to the point of giving very weak gels. On the basis of isothermal titration calorimetry results, it was proposed that HEC did not adsorb onto CNC surfaces and that increased viscosities were due to depletion induced attractive interactions between CNC particles.

Surfactants are present in most formulated chemical products. Although not classical surfactants, Beck-Candanedo reported the influence of ionic dyes on the phase behavior of completely anisotropic dispersions (i.e., CNC concentration > C_2).[31] Cationic and other cellulose adsorptive dyes had no influence on the phase behavior, whereas dyes that remained in solution caused the formation of a coexisting isotropic phase. In other words, C_2 was shifted to much higher CNC concentrations upon introduction of nonadsorbing soluble dyes. Tam's group reported cationic surfactant interactions with both sulfated CNC particles[32] and with CNC particles with grafted polypropylene glycol oligomers.[33] They showed that cationic surfactant strongly binds to sulfated CNC particles; low surfactant dosages caused aggregation whereas colloidally stable cationic CNC particles were obtained with high dosages. Finally, we have found no publications describing the properties of CNC suspensions in mixtures of surfactants with water-soluble polymers—a common situation with formulated products. Herein we report results of an initial investigation that shows the critical feature is whether or not the polysaccharides adsorb onto CNC surfaces.

EXPERIMENTAL SECTION

Materials and Methods. Hydroxypropyl guar (HPG, 2.5× 10^6 Da, degree of substitution (DS) of 0.36) was obtained from Alcon Laboratories (Fort Worth, TX). Sigma-Aldrich provided hydroxyethyl celluloses: HEC250 MW = 250 kDa, DS = 1, and molar substitution (MS) = 2; HEC720 MW = 720 kDa, DS n/a, and MS = 2.5; and, HEC1300 MW = 1300 kDa, DS n/a, and MS = 2.5. Locust beam gum (LBG, 310 kDa), dextran (DEX, 2000 kDa), sodium dodecyl sulfate (SDS), cetyltrimethylammonium bromide (CTAB), poly(ethylene glycol) *p*-(1,1,3,3-tetramethylbutyl)phenyl ether (Triton X-100), HEPES (4-(2-hydroxyethyl)-1-piperazineethanesulfonic acid) buffer, TEMPO (2,2,6,6-tetramethylpiperidin-1-yl)oxidanyl), sodium bromide, and sodium hypochlorite (NaClO, available chlorine, 10−15%) were all obtained from Sigma-Aldrich. The water used in all solutions was deionized and further purified with a Barnstead Nanopure Diamond system (Thermo Scientific, Asheville, NC).

Sulfuric Acid Hydrolysis of Cellulose. Following Revol et al., CNC was prepared by sulfuric acid hydrolysis of cotton from cotton filter aid (Whatman ashless filter aid, GE Healthcare Canada, Mississauga, Canada).[3] 40 g of the filter aid was treated with 700 mL of 64 wt % sulfuric acid (Fischer Scientific) at 45 °C for 45 min with constant stirring (mechanical stirrer) in a water bath. Immediately following the acid hydrolysis, the suspension was diluted 10-fold with water to quench the reaction. The suspension was centrifuged at 6000 rpm for 10 min four times to concentrate the cellulose and to remove excess aqueous acid. The precipitate was then rinsed, centrifuged, and dialyzed against water for 2 weeks until the pH of external dialysis reservoir stabilized. The suspension was sonicated in continuous mode for 30 min (Sonifier 450, Branson Ultrasonics, Danbury, CT) at 50% output while cooling in an ice bath to prevent overheating in order to unhinge any loosely bound CNC particles. Dowex Marathon C hydrogen-form resin (Sigma-Aldrich) was introduced to the cellulose suspension for 48 h and then removed by filtering through hardened ashless filter paper (Whatman 541). The resultant aqueous suspension was approximately 1 wt % cellulose, and the concentration was increased by evaporation at ambient conditions. The surface charge density of CNC was calculated to be 0.16 ± 0.02 mequiv/g as measured by conductometric titration, with average crystal dimensions of 128 × 7 nm from transmission electron microscopy (TEM) images. A small amount of toluene (50 μL per 1 L of suspension) was added to the cellulose suspension to avoid bacterial growth.

Hydrochloric Acid Hydrolysis of Cellulose and TEMPO Oxidation. 10 g of the cotton filter aid was hydrolyzed with 2.5 M HCl at 70 °C for 2 h as described by Kalashnikova et al.[6] Acid was removed by successive centrifugations at 6000 rpm for 10 min and redispersion of the solid materials in purified water until pH was above 5. The resultant precipitate was then dialyzed against water for 2 weeks to remove any remaining contaminants, deionized by mixing with mixed bed ion-exchange resin, and concentrated to constitute the stock suspension, which was used to prepare oxidized cellulose

dx.doi.org/10.1021/la404977t | Langmuir 2014, 30, 2684−2692

nanocrystals. Oxidation experiments were carried out as previously published with minor modifications.[34] 10 mg of TEMPO and 200 mg of sodium bromide were added while magnetically stirring the cellulose suspension (60 mL of 1 wt %) that had previously been sonicated for 3 min. The TEMPO-mediated oxidation of the cellulose nanocrystals was initiated by slowly adding 4.9 mL of NaClO over 20 min at room temperature under stirring. The reaction pH was maintained constant at 10 by adding 1 M NaOH solution until the pH was stable, indicating that the reaction was finished. About 5 mL of methanol was then added to quench the extra oxidant. After adjusting the pH to 7 by adding 1 M HCl, the TEMPO-oxidized product was rinsed with purified water by centrifugation and further purified by dialysis against water for a week. The carboxylic content in the oxidized cellulose nanocrystals, with average dimensions of 119 × 8 nm from TEM images, was determined to be 0.20 ± 0.04 mequiv/g by conductometric titration.

Conductometric Titration. Titrations were performed using a Burivar-I2 automatic buret (ManTech Associates) as described previously on both sulfated and carboxylated CNC to determine the charge content of the suspensions. 50 g portions of 0.5 wt % CNC suspensions in 1 mM KCl was titrated using slow base-into-acid titrations (30 min/unit pH).

Electrophoretic Mobility. Electrophoretic mobility values were measured using a ZetaPlus analyzer (Brookhaven Instruments Corp.) operating in phase analysis light scattering mode. A total of 10 runs (each composed of 15 cycles) were conducted; the experimental uncertainties represent the standard error of the mean of the replicate runs. The CNC and polymer concentrations were kept 0.4 wt % and 1 g/L, respectively. SDS, CTAB, and Triton X-100 were later added to CNC suspensions that had been previously mixed with polymer solutions and concentrations of the surfactants were kept 10, 2, and 2 mM, respectively.

Dynamic Light Scattering. Measurement were made using a Brookhaven BI-APD dynamic light scattering apparatus with a detector angle of 90°. A Melles Griot HeNe operating at a wavelength of 633 nm was used as the light source. The scattering intensity was between 100 and 250 kcps for all measurements. Each sample was measured for three runs with 3 min for each run. The results were analyzed using a BI-9000AT digital autocorrelator, version 6.1 (Brookhaven Instruments Corp.), and the CONTIN statistical method was used to calculate the particle size distribution.

Preparation of CNC-Coated Sensors. TiO_2 SPR sensors (Bionavis) and silica QCM-D sensors (Q-Sense AB) were cleaned by dipping in ethanol, rinsing with purified water, and drying with nitrogen gas followed by UV/ozone treatment for 15 min. The silica QCM-D sensors were spin-coated at 3000 rpm for 60 s, with a layer of 1.0 g/L polyvinylamine (PVAm), M_w = 45 kDa (BASF, Ludwigshafen, Germany) as the adhesive layer. Excess, unadsorbed PVAm was removed by washing with water. Next, the CNC suspension (2 wt %) was spin-coated onto the substrates at 3000 rpm for 60 s. To ensure that the spin-coated films did not desorb in water, they were heat-treated in an oven at 80 °C for 2 h, rinsed with purified water, and dried with N_2 gas. Some CNC desorption was observed with shorter (15 min) heating times. The same procedure was followed to spin-coat TiO_2 SPR sensors with a CNC film. However, the adhesive layer of PVAm was not required for coating on the cationic TiO_2 SPR sensors.

Quartz Crystal Microbalance with Dissipation Monitoring (QCM-D). Adsorption measurements were performed with an E4 QCM-D instrument from Q-Sense AB (Sweden) where the third, fifth, and seventh overtones were recorded. QCM-D measures the damping of the crystal oscillation (the dissipation factor D) in addition to the frequency shift (Δf) of a quartz crystal sensor in contact with an adsorbing medium. All the data were normalized to the fundamental frequency by dividing the result with the overtone number (3). Before the adsorption experiments, all CNC-coated QCM-D sensors were soaked in purified water overnight. All experiments were performed at 23 °C, using HEPES buffer solutions (150 mM, pH 7.4).

For each adsorption experiment, the sequence of injections was identical: (1) an aqueous solution of HEPES buffer was injected at a constant flow rate of 150 μL/min until the baseline frequency shift was less than 0.5 Hz over 10 min; (2) the 1 g/L hydroxyethyl cellulose (HEC), hydroxypropyl guar (HPG), locust bean gum (LBG), or dextran (DEX) in HEPES buffer were injected at 150 μL/min until the baseline was again stable, typically after 30 min; (3) the samples were rinsed with HEPES buffer at 150 μL/min until the baseline was stable, typically after 5 min.

Surface Plasmon Resonance (SPR) Measurements. SPR experiments were performed using the SPR Navi200 (Bionavis, Finland) at 23 °C. An increase in layer thickness adsorbed on the SPR sensor produces a shift in optical resonance properties of the sensor. This shift is detected as an increase in the SPR angle (θ_{peak}) where the reflected light intensity is minimized.[35] Reflected intensity as a function of incident angle was collected over the angular range of 40°−80° such that the SPR angle position and the angle of total internal reflectance (θ_{tir}) were both detected. The θ_{tir} is related to the refractive index of the surrounding medium, and if the medium changes, θ_{tir} shifts and the SPR angle shifts by the same amount. As such, it is important to subtract θ_{tir} from the SPR peak angle to ensure that measured angular shifts are due to adsorbed material alone and not to media effects. SPR sensorgrams are presented as $\Delta\theta_{peak}-\Delta\theta_{tir}$ as a function of adsorption time. All SPR measurements were performed using 670 and 785 nm wavelengths for the bare sensor surfaces and the CNC-coated sensor surface before and after polymer adsorption. Polysaccharide solutions were introduced at 100 μL/min.

The SPR data (full angular scans from 40° to 80°) were simulated using Winspall 3.02 (Max-Planck Institute for Polymer Research Mainz, Germany). This model treats the surface as a uniform slab and yields plots of slab thickness versus refractive index. By making independent measurements at two wavelengths, it is possible to estimate a unique combination of slab thickness and refractive index.[36] Details of the method and optical constants are given in the Supporting Information.

For polymer desorption experiments as a result of surfactant addition, the sequence of injections was identical: (1) an aqueous solution of HEPES buffer was injected at a constant flow rate of 100 μL/min until the baseline $\Delta\theta_{peak}-\Delta\theta_{tir}$ shift was less than 0.005 over 5 min; (2) the 1 g/L hydroxyethyl cellulose (HEC, M_w = 250 kDa) was injected at 100 μL/min until the baseline was again stable, typically after 20 min; (3) the samples were rinsed with HEPES buffer at 100 μL/min until the baseline was stable, typically after 5 min; (4) SDS (10 mM in HEPES buffer), CTAB (2 mM in HEPES buffer), or Triton X-100 (2 mM in HEPES buffer) was injected at 100 μL/min until the baseline was again stable, typically after 20 min; (5) the samples were rinsed with HEPES buffer at 100 μL/min until the baseline was stable, typically after 10 min.

Gelation Tests. Equal volumes of CNC suspensions (ranging from 0.5 to 20 wt %) and each polysaccharide solution (in 300 mM HEPES buffer) with different concentrations were mixed together, and gelation was assessed by a modified test tube inversion method. Specifically, if no liquid accumulation was observed on the bottom of the inverted vial/tube 30 min after mixing of polymers and CNC suspensions, it was concluded that a gel had formed. Some HEC−CNC gels were treated with surfactants. Equal volumes of surfactant solution (SDS, CTAB, or Triton X-100) were combined and immediately vortexed. The tube inversion tests were repeated as before to determine the effects of surfactant addition on gelation. The final concentrations of SDS, CTAB, and Triton X-100 in the samples were kept to 10, 2, and 2 mM, respectively.

Rheology. Storage (G') and loss moduli (G'') were measured using a CC25 concentric cylinder cell with a sample volume of 16 mL of an STRESSTECH HR ATS rheometer (Rheologica Instruments) at 21 °C. A strain sweep was first performed to identify the linear viscoelastic range of each hydrogel composite, followed by a frequency sweep over the range of 0.01−10 rad/s to determine the shear-dependent complex viscosity, G', and G'' of the hydrogels. An example strain sweep is shown in Figure SI 13 of the Supporting Information.

Polarized Optical Microscopy (POM). Color micrographs were obtained using a Nikon Eclipse LV100POL microscope with a 530 nm phase retardation plate. With the retardation plate, isotropic areas appear dark pink and oriented regions, either blue or yellow, the

dx.doi.org/10.1021/la404977t | Langmuir 2014, 30, 2684−2692

difference being a 90° in-plane rotation of the sample alignment direction. Digital images were taken of samples in rectangle hollow capillary tubes (VitroCom, Mountain Lakes, NJ).

RESULTS

Interactions of Water-Soluble Nonionic Polysaccharides with CNC Surfaces. CNC dispersions were prepared by conventional sulfuric acid hydrolysis, yielding average crystal dimensions of 128 nm × 7 nm and a charge content of 0.16 ± 0.02 mequiv/g. For a few experiments, carboxylated cellulose nanocrystals (CNC-COOH) were also prepared,[6] producing particles with average dimensions of 119 nm × 8 nm and a charge content of 0.20 ± 0.04 mequiv/g. TEM micrographs and example conductometric titrations are shown in Figures SI-1 and SI-2, respectively. Many of the measurements reported in this paper were performed in 150 mM HEPES buffer at pH 7.2. Compared to the conditions used for many of the classic CNC studies, this is a high ionic strength that was chosen to more closely mimic conditions in commercial formulated aqueous products. Pristine sulfated CNC is electrostatically stabilized, and DLS measurements indicated some aggregation in HEPES buffer concentrations greater than 100 mM (see Figure SI-3).

The interactions of four polysaccharide types with CNC surfaces were probed by dynamic light scattering (DLS), microelectrophoresis, QCM-D, and SPR. In all cases the results suggest HEC, hydroxypropyl guar (HPG), and locust bean gum (LBG) adsorb onto cellulose in 150 mM HEPES buffer, whereas DEX does not. For example, Table 1 shows that DEX had little influence on CNC apparent diameter, whereas the other three polymers induced a substantial increase in the apparent size of the CNC crystals. Note the apparent diameters were based on sphere models that do not account for the particle shape. DLS measurements in the presence of the remaining polysaccharides and varying ionic strengths are shown in the Supporting Information (Figure SI-3), and these results are consistent with the adsorption of all polymers except DEX.

Table 1. Electrophoretic Mobility (EM) and Apparent Diameter of 0.04 wt % CNC Dispersions in the Presence of 0.1 g/L Polysaccharides and Surfactants[a]

additive	CNC EM 10^{-8} m^2/(V s)	apparent diameter (nm)
no additive	−2.56 ± 0.21	113 ± 10
DEX	−2.29 ± 0.18	111 ± 10
HPG		300 ± 28
LBG		218 ± 20
HEC1300		269 ± 25
HEC720		228 ± 20
HEC250	−0.11 ± 0.07	190 ± 18
HEC250 + SDS 10 mM	−2.34 ± 0.06	
HEC250 + CTAB 2 mM	0.19 ± 0.16	
HEC250 + T. X-100 2 mM	−2.22 ± 0.19	

[a]Apparent diameters were based on the Stokes law conversion of diffusion coefficients obtained by DLS using the CONTIN analysis. The error estimates are the standard error of the mean apparent hydrodynamic diameter of three runs of each sample.

The electrophoretic mobilities of dilute CNC in 2 mM NaCl with and without polysaccharides are summarized in Table 1. Without polymers, the mobility is highly negative, reflecting the high surface charge density of sulfate half-ester groups. Again, we see that in the presence of DEX the mobility was slightly decreased, whereas in HEC, LBG, and HPG, the mobility was substantially lower because adsorbed polymer shifted the shear plane away from the highly charged CNC surfaces.

Adsorption measurements were performed with a quartz crystal microbalance with dissipation (QCM-D) and surface plasmon resonance (SPR) spectroscopy using sensor surfaces spin-coated with CNC. Figure 2 shows QCM-D frequency shift results from the introduction of the four polysaccharides. HEC, LBG, and HPG gave a large frequency drop, suggesting adsorption, whereas DEX did not. This series of experiments was repeated with QCM-D sensors coated with carboxylated cellulose nanocrystals, CNC-COOH, and the results in Figure SI-7 show similar results, but with slightly lower adsorbed masses.

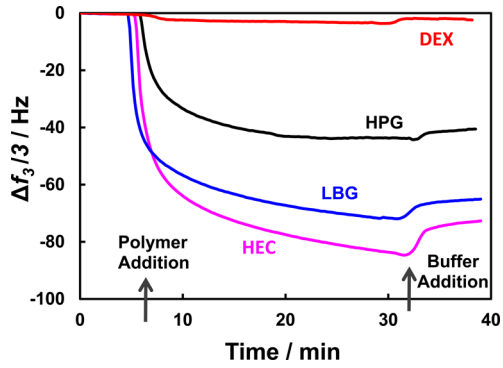

Figure 2. $\Delta f_3/3$ versus time for QCM-D studies of sulfated CNC-coated silica sensors exposed to HEC1300, LBG, HPG, and DEX solutions (1 g/L in 150 mM HEPES buffer at pH 7.2). $\Delta f_3/3$, the frequency drop normalized by the overtone, is a measure of the adsorbed mass including bound water.

The corresponding dissipation results (see Figure SI-6) show significant viscoelastic behavior, indicating highly associated water contents for the adsorbed polymers and thus precluding the use of the Sauerbrey model for predicting adsorbed amounts. Thus, it is not possible from these results to rank the relative adsorbed amounts of HPG, LBG, and HEC. On the other hand, it is clear that DEX did not adsorb; presumably, DEX adsorption onto cellulose is energetically unfavorable.

SPR adsorption measurements were performed to obtain adsorbed layer thickness values for the HEC samples. Our SPR instrument performed simultaneous measurements at two wavelengths, permitting the estimation of the adsorbed layer thickness values. The analyses, including the optical constants, are described in the Supporting Information. The resulting estimates of adsorbed layer thickness values are plotted as a function of the square root of the HEC molecular weight in Figure 3. In view of the complexity of the samples, we consider these thickness results to be semiquantitative. Nevertheless, the adsorbed layer thickness values, estimated from SPR measurements, were proportional to the square root of the molecular weight. Also shown in Figure 3 are adsorbed layer values from a model—these results are explained in the Discussion section.

Influence of Water-Soluble Nonionic Polysaccharides on Gelation. Initial experimentation showed that very low concentrations of some nonionic, water-soluble polysaccharides could induce CNC suspension gelation. CNC gelation was assessed by simple vial inversion tests. Gels that did not move when the vials were inverted are classified as "invertible gels". Figure 4 shows that 3 wt % CNC suspensions formed gels

dx.doi.org/10.1021/la404977t | Langmuir 2014, 30, 2684−2692

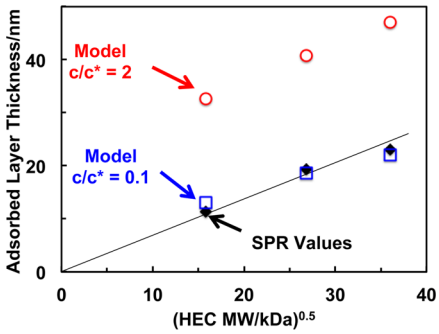

Figure 3. Influence of HEC molecular weight on the estimated adsorbed thickness on CNC-coated substrates in 150 mM HEPES buffer at pH 7.2. The model results are explained in the Discussion section.

when mixed with only 0.2 wt % LBG, HPG, or HEC. By contrast, DEX did not induce formation of an invertible gel.

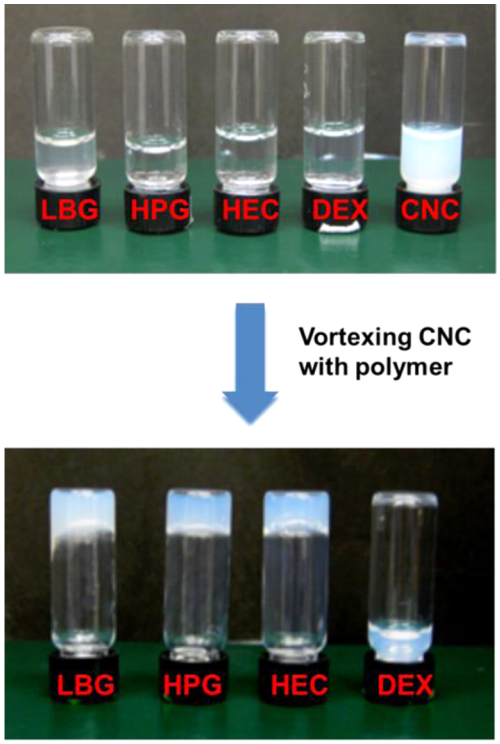

Figure 4. Photographs of polysaccharide solutions before and after vortex mixing with CNC suspensions. Only the dextran (DEX) did not induced gelation. The final suspensions were 3 wt % CNC + 0.2 wt % polysaccharide in 150 mM HEPES buffer at pH 7.2. The HEC was HEC1300 (see Table 1).

Gel formation was further demonstrated by rheological measurements. HEC−CNC mixtures showed classic gel behavior with $G' > G''$ and a rather flat frequency response. HPG or LBG with CNC showed similar behaviors (Figure SI-4). By contrast, with DEX−CNC mixtures, $G'' > G'$, which is typical behavior for polymer solutions. The corresponding curves made with carboxylated CNC−COOH showed similar behavior (see Figure SI-5).

Polarized optical microscopy (POM) and transmission electron microscopy (TEM) images of polymer−CNC samples are shown in Figure 5. LBG−CNC, HPG−CNC, and HEC−CNC samples demonstrated anisotropic regions in both POM and TEM images, whereas the DEX−CNC sample only showed random ordering of the CNC particles.

Figure 6 further illustrates the ability of HEC to induce CNC gelation. The *Y*-axis shows the minimum CNC volume fraction required to form a gel as judged by the vial inversion tests. The *X*-axis shows the polymer concentration divided by *C**, which is the polymer concentration corresponding to the dilute-to-semidilute transition (overlap concentration). At concentrations as low as 1/10th *C**, all three HEC molecular weights lowered the CNC gelation concentration by an order of magnitude. In addition, the higher the HEC molecular weight, the more dramatic the effect on gelation. Note that without polymer the CNC concentration for invertible gel formation was about 15 vol % and that none of the polymers gave invertible gels at the concentrations we evaluated. Therefore, gelation depended upon HEC/CNC interactions.

Surfactant Interaction of CNC−HEC Gels. In addition to water-soluble polymers, most formulated products contain surfactants. We mixed three typical surfactants, at concentrations slightly above their critical micelle concentrations, with HEC−CNC gels. Anionic SDS and nonionic Triton X-100 destroyed the uniform gels, giving visible CNC precipitates immediately after mixing. By contrast, cationic CTAB did not disrupt the gel. POM micrographs (Figure SI-12) indicated the presence of ordered domains in the samples after the addition of all three surfactants. The electrophoresis results in Table 1 show that addition of SDS or Triton X-100 to CNC−HEC mixtures increases the negative electrophoretic mobility back to values close to CNC without polymers. By contrast, CTAB absorption gives charge reversal. In the Discussion section we argue that that SDS and Triton X-100 disrupted the adsorbed HEC and thus led to gel breaking.

Further support for the proposal that SDS and Triton induce HEC desorption from CNC is given in Figure 7. SDS and Triton X-100 induced partial desorption (~70%) of the adsorbed HEC with most desorption occurring during the final buffer rinse. This is a reproducible observation for which we have no explanation. In contrast to the behaviors in SDS and Triton X-100, exposure to cationic CTAB increased the amount of material adsorbed on the cellulose. We presume the additional adsorbed material is CTAB; however, this remains to be proven. These results highlight the complexities of mixing CNC with polymers and surfactants.

■ DISCUSSION

In this work we have focused on factors influencing gelation of CNC suspensions with particular emphasis on whether or not the inverted gels flow. Without added polymer our CNC gels did not flow when inverted if the volume fraction of CNC was ≥14% (see Figure 6). A 14 vol % suspension corresponds to 19.6 wt % CNC, and a number concentration of $\sim 14 \times 10^{-6}$ nm^{-3}. This number concentration is within the range of CNC concentrations reported by Dong et al.[17] for suspensions with an anisotropic volume fraction of 100% (i.e., no coexisting isotropic phase).

Our results show that three of four nonionic, water-soluble polysaccharides greatly lower the CNC concentration required for invertible gel formation. On the other hand, two of three common surfactant types disrupt HEC−CNC gels. These sensitivities of CNC dispersions have serious implications for CNC formulation into water-based products because such polysaccharides are frequently used to control viscosity. The

dx.doi.org/10.1021/la404977t | *Langmuir* 2014, 30, 2684−2692

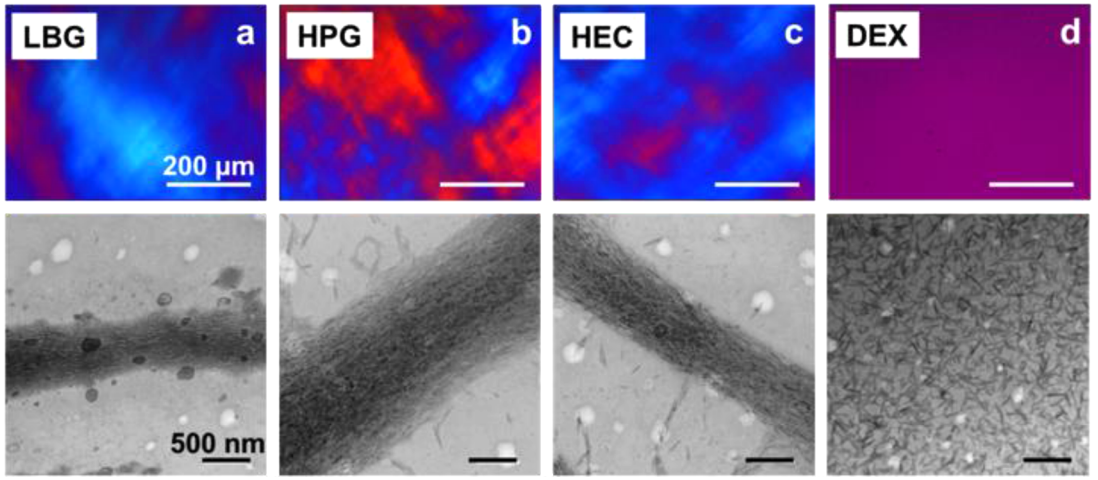

Figure 5. Polarized optical micrographs (POM; top panel) and transmission electron micrographs (TEM; bottom panel) of CNC (3 wt %) suspensions in the presence of polysaccharides (0.2 wt %) in 150 mM HEPES buffer at pH 7.2.

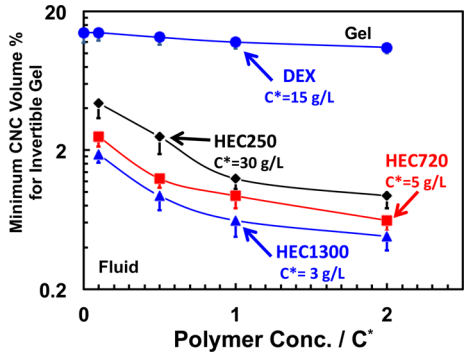

Figure 6. Minimum CNC volume percent for gelation (inversion test) as a function of the polysaccharide concentration in 150 mM HEPES buffer at pH 7.2. C*, the overlap concentrations, were from the literature.[28,37]

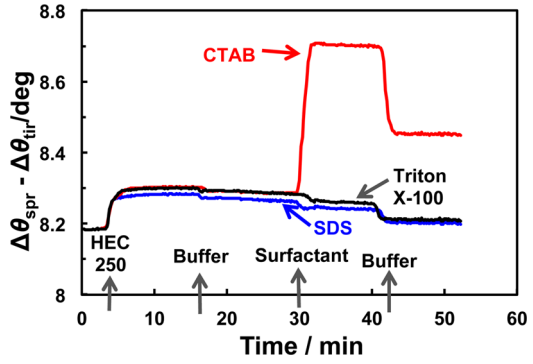

Figure 7. Influence of surfactants on HEC250 adsorbed from a 1 g/L solution onto a CNC-coated SPR sensor (data collected at 785 nm). The surfactant concentrations were SDS 10 mM, CTAB 2 mM, and Triton X-100 2 mM. All measurements were made in 150 mM HEPES buffer at pH 7.2.

ability of hydrophilic polysaccharides to influence rheology and colloidal stability has been discussed in many other systems, and generally most effects are explained by depletion flocculation.[38] The following paragraphs make the case that depletion effects (and bridging) are not dominant in our system.

Addition of HEC to CNC suspensions at concentrations as low as 1/10th C*, the overlap concentration, induced gelation, whereas dextran had little influence (see Figure 6). The polymer concentrations were in the dilute regime (i.e., <C*), suggesting that depletion forces were not responsible for the invertible gel formation.

The QCM-D, SPR, electrophoresis, and dynamic light scattering results showed HEC, HPG, and LBG adsorbed onto CNC surfaces, whereas DEX did not. Therefore, the ability of polymers to induce CNC gelation was correlated with the tendency of the polymers to adsorb onto CNC. These results were surprising to us as HEC is widely used as a thickener in aqueous dispersions because it does not adsorb onto many surfaces. There are few publications describing HEC interactions with cellulose. Boluk's isothermal titration calorimetry experiments failed to measure heat effects associated with HEC interaction with CNC.[28] Berglund's group has shown that nanocellulose/HEC blends form tough dry composites suggesting adhering interfaces between HEC and cellulose.[39] In summary, we are confident that HEC adsorption on our CNC-coated surfaces was not an artifact because the QCM-D and SPR coated sensors were prepared with different adhesive layers (polyvinylamine for the QCM-D and no adhesive layer on TiO_2 for SPR) and the CNC layer was thick enough to avoid substrate effects. Furthermore, both the microelectrophoresis and DLS results suggest HEC adsorption onto CNC. Assuming that our adsorption measurements reflect adsorption onto dispersed CNC particles, the role of polysaccharide adsorption on CNC gelation is now considered.

The simultaneous adsorption of polymer molecules onto two or more particles gives bridging structures and thus could explain gelation. However, a common feature of bridging is that it is not operative at high polymer concentrations. Instead, at high polymer/surface area ratios, all surfaces are saturated with adsorbed polymer giving steric stabilization. Our gelation results in Figure 6 show no evidence of a bridging-to-steric stabilization transition at high polymer concentrations. Therefore, we do not believe bridging interactions explain the polysaccharide-induced gelation. Instead, we propose that HEC lowers the CNC concentration for gelation by adsorbing onto the particles, increasing the effective volume fraction of CNC particles. The following model illustrates the roles of polymer adsorption and volume fraction.

dx.doi.org/10.1021/la404977t | Langmuir 2014, 30, 2684−2692

A gelation model requires a criterion for the onset of gelation. For example, Philipse's review discusses the criteria for gelation of nonadhering and adhering rod suspensions.[40] For simplicity, we assume that an invertible gel forms at the CNC concentration = C_2 and $\phi = \phi_a = 1$, the lowest CNC concentration at which the suspension is entirely anisotropic (see Figure 1). Although reasonable, we emphasize this assumption is arbitrary. The effective volume fraction of a suspension of rectangular particles of width W = 7 nm with an adsorbed polymer layer thickness δ is given by eq 1, where c is the mass fraction of cellulose in the suspension, ρ_w is the density of water, and, ρ_{CNC} = 1600 kg/m^3 is the density of cellulose. Note this expression ignores the contribution of polymer adsorbed on the ends of the particles.

$$\phi = \frac{\rho_w}{\left(\frac{1}{c} - 1\right)\rho_{CNC} + \rho_w} \frac{(W + 2\delta)^2}{W^2} \quad (1)$$

We applied eq 1 to the results in Figure 6 to estimate the corresponding δ values. The experimental cellulose volume fractions in Figure 6 were converted to the corresponding mass fractions, c, and eq 1 was solved numerically for δ values, setting ϕ = 1. The calculations, performed with Mathcad, are listed in the Supporting Information. Polymer adsorbed layer thickness values, δ, were calculated for c values corresponding to both the lowest and highest experimental HEC concentrations in Figure 6. The resulting thickness values are compared to the SPR experimental values in Figure 3. The computed thickness corresponding to the low polymer concentrations are very close to the experimental SPR values, whereas those for the high polymer concentration data are about 2 times greater than the experimental values. In summary, this simple model simulated the major features of gelation results, giving support to our proposal that HEC, HPG, and LBG induced gelation because the polymer adsorbed on the CNC surfaces, increasing the effective volume fraction.

If we accept that HEC adsorption explains enhanced gelation of CNC dispersions, it seems reasonable to propose that subsequent SDS or Triton X-100 addition induced HEC desorption. The literature teaches that the anionic surfactant SDS[41] and the nonionic Triton X-100[42] do not bind to HEC in solution. On the other hand, the adsorption of an anionic surfactant, sodium dodecylbenzenesulfonate (NaDBS), and a nonionic surfactant, Triton X-100, on cellulose surfaces with and without electrolytes has been reported.[43] Both our SPR (Figure 7) and microelectrophoresis (Table 1) results together with the literature support the proposition that SDS and Triton X-100 adsorb on CNC surfaces, displacing the adsorbed HEC layer. Furthermore, the photographs in Figure SI-12 of the Supporting Information show that SDS and Triton X-100 induced some aggregation, possibly because of depletion flocculation. By contrast, CTAB, the cationic surfactant, showed very different behavior.

The results in Figure 7 show a surface mass increase when HEC-treated cellulose is exposed to CTAB. It is not known whether CTAB simply adds to the layer or displaces some of the HEC. However, since there is no destruction of the invertible gel, we propose that CTAB penetrates the HEC layers, binding to the negatively charged CNC surfaces with little change to the effective volume fraction of the coated particles. In addition, electrophoretic mobility measurements (Table 1) of CNC suspensions that have been previously mixed with HEC were positively charged and colloidally stable. Though HEC-free CNC suspension in 2 mM CTAB was also positively charged (EM = $(0.68 \pm 0.12) \times 10^{-8}$ m^2/(V s)), the dispersion was unstable and aggregated 1 h after mixing CNC with CTAB. The sample of HEC−CNC−CTAB, on the other hand, showed no sign of aggregation three days after preparation, presumably because adsorbed HEC served as a steric stabilizer.

Finally, formulators have hundreds of water-soluble polymers and thousands of surfactants from which to choose. Obviously, this work involves a limited subset of the formulation landscape. Our nonionic polysaccharides are particularly benign because they are very hydrophilic and thus are weakly interacting in water both with surfaces and surfactants. Nevertheless, we have demonstrated a complex range of behaviors. More hydrophobic and/or charged polymers are likely to display more dramatic interactions with CNC and with any surfactants present.

CONCLUSIONS

Gelation of dilute CNC suspensions was induced by the introduction of the nonionic polysaccharides HEC, HPG, and LBG, whereas DEX has no influence on gelation. The ability of a polysaccharide to induce gelation directly correlates with the tendency of the polymer to adsorb on the CNC surfaces. Absorbing polymers dramatically increase the effective volume fraction of CNC dispersions, driving them into a completely anisotropic phase with a sufficient yield stress to not flow when inverted. Addition of surfactants to HEC−CNC invertible gels gave a range of behaviors depending upon the nature of the surfactant. Anionic SDS and nonionic Triton X-100 decompose the gels inducing HEC desorption from CNC surfaces, whereas gels were preserved in the presence of CTAB. This work emphasizes that although CNC is potentially a potent ingredient for promoting weak gel formation in formulated chemical products, the detailed behaviors are very sensitive to the presence of water-soluble polymers and surfactants.

ASSOCIATED CONTENT

Supporting Information

Transmission electron microscopy (TEM), conductometric titration, dynamic light scattering (DLS), rheology data corresponding to the results in Figure 5, quartz crystal microbalance with dissipation monitoring (QCM-D) data corresponding to the results in Figure 2, surface plasmon resonance (SPR) data and simulation example corresponding to the results in Figure 3, atomic force microscopy (AFM) data, and a copy of the MathCad model used to perform the calculation of volume fraction increase due to the adsorption of polymer. This material is available free of charge via the Internet at http://pubs.acs.org.

AUTHOR INFORMATION

Corresponding Author

*E-mail: peltonrh@mcmaster.ca (R.P.).

Notes

The authors declare no competing financial interest.

ACKNOWLEDGMENTS

The authors thank Sarah Ballinger and Kevin Kan for CNC preparation, Elizabeth Takacs and Roozbeh Mafi for rheometry support, and Heera Marway for SPR support. Tiffany Abitbol is thanked for sample analysis with POM and AFM. The

McMaster Biointerfaces Institute is acknowledged for access to instrumentation. Hu thanks NSERC for funding this work through the CREATE Biointerfaces Training Program Grant. Pelton holds the Canada Research Chair in Interfacial Technologies.

REFERENCES

(1) Ranby, B. G Aqueous Colloidal Solutions of Cellulose Micelles. *Acta Chem. Scand.* **1949**, *3*, 649−650.
(2) Klemm, D.; Kramer, F.; Moritz, S.; Lindstrom, T.; Ankerfors, M.; Gray, D.; Dorris, A. Nanocelluloses: A New Family of Nature-Based Materials. *Angew. Chem., Int. Ed.* **2011**, *50*, 5438−5466.
(3) Revol, J. F.; Bradford, H.; Giasson, J.; Marchessault, R. H.; Gray, D. G. Helicoidal Self-Ordering of Cellulose Microfibrils in Aqueous Suspension. *Int. J. Biol. Macromol.* **1992**, *14*, 170−172.
(4) Espinosa, S. C.; Kuhnt, T.; Foster, E. J.; Weder, C. Isolation of Thermally Stable Cellulose Nanocrystals by Phosphoric Acid Hydrolysis. *Biomacromolecules* **2013**, *14*, 1223−1230.
(5) Cao, X.; Dong, H.; Li, C. M. New Nanocomposite Materials Reinforced with Flax Cellulose Nanocrystals in Waterborne Polyurethane. *Biomacromolecules* **2007**, *8*, 899−904.
(6) Kalashnikova, I.; Bizot, H.; Cathala, B.; Capron, I. New Pickering Emulsions Stabilized by Bacterial Cellulose Nanocrystals. *Langmuir* **2011**, *27*, 7471−7479.
(7) Rincon-Torres, M. T.; Hall, L. J. Cellulose Nanowhiskers in Well Services. US Patent App. 13/561,158, 2012.
(8) Kan, K. H. M.; Li, J.; Wijesekera, K.; Cranston, E. D. Polymer-Grafted Cellulose Nanocrystals as pH-Responsive Reversible Flocculants. *Biomacromolecules* **2013**, *14*, 3130−3139.
(9) Boluk, Y.; Lahiji, R.; Zhao, L.; Mcdermott, M. T. Suspension Viscosities and Shape Parameter of Cellulose Nanocrystals (Cnc). *Colloids Surf., A* **2011**, *377*, 297−303.
(10) Zhong, L.; Fu, S.; Peng, X.; Zhan, H.; Sun, R. Colloidal Stability of Negatively Charged Cellulose Nanocrystalline in Aqueous Systems. *Carbohydr. Polym.* **2012**, *90*, 644−649.
(11) Revol, J. F.; Godbout, L.; Gray, D. G. Solid Self-Assembled Films of Cellulose with Chiral Nematic Order and Optically Variable Properties. *J. Pulp Paper Sci.* **1998**, *24*, 146−149.
(12) Fall, A. B.; Lindstrom, S. B.; Sundman, O.; Odberg, L.; Wagberg, L. Colloidal Stability of Aqueous Nanofibrillated Cellulose Dispersions. *Langmuir* **2011**, *27*, 11332−11338.
(13) Araki, J.; Wada, M.; Kuga, S. Steric Stabilization of a Cellulose Microcrystal Suspension by Poly(Ethylene Glycol) Grafting. *Langmuir* **2001**, *17*, 21−27.
(14) Onsager, L. The Effects of Shape on the Interaction of Colloidal Particles. *Ann. N. Y. Acad. Sci.* **1949**, *51*, 627−659.
(15) Flory, P. J. Statistical Thermodynamics of Mixtures of Rodlike Particles. 5. Mixtures with Random Coils. *Macromolecules* **1978**, *11*, 1138−1141.
(16) Stroobants, A.; Lekkerkerker, H. N. W.; Odijk, T. Effect of Electrostatic Interaction on the Liquid Crystal Phase Transition in Solutions of Rodlike Polyelectrolytes. *Macromolecules* **1986**, *19*, 2232−2238.
(17) Dong, X. M.; Kimura, T.; Revol, J. F.; Gray, D. G. Effects of Ionic Strength on the Isotropic-Chiral Nematic Phase Transition of Suspensions of Cellulose Crystallites. *Langmuir* **1996**, *12*, 2076−2082.
(18) Dong, X. M.; Gray, D. G. Effect of Counterions on Ordered Phase Formation in Suspensions of Charged Rodlike Cellulose Crystallites. *Langmuir* **1997**, *13*, 2404−2409.
(19) Odijk, T. Theory of Lyotropic Polymer Liquid Crystals. *Macromolecules* **1986**, *19*, 2313−2329.
(20) Wierenga, A. M.; Philipse, A. P. Low-Shear Viscosity of Isotropic Dispersions of (Brownian) Rods and Fibres; a Review of Theory and Experiments. *Colloids Surf., A* **1998**, *137*, 355−372.
(21) Araki, J.; Wada, M.; Kuga, S.; Okano, T. Flow Properties of Microcrystalline Cellulose Suspension Prepared by Acid Treatment of Native Cellulose. *Colloids Surf., A* **1998**, *142*, 75−82.
(22) Bercea, M.; Navard, P. Shear Dynamics of Aqueous Suspensions of Cellulose Whiskers. *Macromolecules* **2000**, *33*, 6011−6016.
(23) Liu, D.; Chen, X.; Yue, Y.; Chen, M.; Wu, Q. Structure and Rheology of Nanocrystalline Cellulose. *Carbohydr. Polym.* **2011**, *84*, 316−322.
(24) Ureña-Benavides, E. E.; Ao, G.; Davis, V. A.; Kitchens, C. L. Rheology and Phase Behavior of Lyotropic Cellulose Nanocrystal Suspensions. *Macromolecules* **2011**, *44*, 8990−8998.
(25) Edgar, C. D.; Gray, D. G. Influence of Dextran on the Phase Behavior of Suspensions of Cellulose Nanocrystals. *Macromolecules* **2002**, *35*, 7400−7406.
(26) Beck-Candanedo, S.; Viet, D.; Gray, D. G. Induced Phase Separation in Low-Ionic-Strength Cellulose Nanocrystal Suspensions Containing High-Molecular-Weight Blue Dextrans. *Langmuir* **2006**, *22*, 8690−8695.
(27) Beck-Candanedo, S.; Viet, D.; Gray, D. G. Triphase Equilibria in Cellulose Nanocrystal Suspensions Containing Neutral and Charged Macromolecules. *Macromolecules* **2007**, *40*, 3429−3436.
(28) Boluk, Y.; Zhao, L.; Incani, V. Dispersions of Nanocrystalline Cellulose in Aqueous Polymer Solutions: Structure Formation of Colloidal Rods. *Langmuir* **2012**, *28*, 6114−6123.
(29) Persson, B.; Nilsson, S.; Sundelöf, L.-O. On the Characterization Principles of Some Technically Important Water-Soluble Nonionic Cellulose Derivatives. Part II: Surface Tension and Interaction with a Surfactant. *Carbohydr. Polym.* **1996**, *29*, 119−127.
(30) Sperry, P. R. A Simple Quantitative Model for the Volume Restriction Flocculation of Latex by Water-Soluble Polymers. *J. Colloid Interface Sci.* **1982**, *87*, 375−384.
(31) Beck-Candanedo, S.; Viet, D.; Gray, D. G. Induced Phase Separation in Cellulose Nanocrystal Suspensions Containing Ionic Dye Species. *Cellulose* **2006**, *13*, 629−635.
(32) Dhar, N.; Au, D.; Berry, R. C.; Tam, K. C. Interactions of Nanocrystalline Cellulose with an Oppositely Charged Surfactant in Aqueous Medium. *Colloids Surf., A* **2012**, *415*, 310−319.
(33) Peng, B.; Han, X.; Liu, H.; Berry, R. C.; Tam, K. C. Interactions between Surfactants and Polymer-Grafted Nanocrystalline Cellulose. *Colloids Surf., A* **2013**, *421*, 142−149.
(34) Filpponen, I.; Argyropoulos, D. S. Regular Linking of Cellulose Nanocrystals via Click Chemistry: Synthesis and Formation of Cellulose Nanoplatelet Gels. *Biomacromolecules* **2010**, *11*, 1060−1066.
(35) Liang, H.; Miranto, H.; Granqvist, N.; Sadowski, J. W.; Viitala, T.; Wang, B.; Yliperttula, M. Surface Plasmon Resonance Instrument as a Refractometer for Liquids and Ultrathin Films. *Sens. Actuators, B* **2010**, *149*, 212−220.
(36) Grassi, J. H.; Georgiadis, R. M. Temperature-Dependent Refractive Index Determination from Critical Angle Measurements: Implications for Quantitative Spr Sensing. *Anal. Chem.* **1999**, *71*, 4392−4396.
(37) Ioan, C. E.; Aberle, T.; Burchard, W. Light Scattering and Viscosity Behavior of Dextran in Semidilute Solution. *Macromolecules* **2001**, *34*, 326−336.
(38) Kiratzis, N.; Faers, M.; Luckham, P. F. Depletion Flocculation of Particulate Systems Induced by Hydroxyethylcellulose. *Colloids Surf., A* **1999**, *151*, 461−471.
(39) Sehaqui, H.; Zhou, Q.; Berglund, L. A. Nanostructured Biocomposites of High Toughness-a Wood Cellulose Nanofiber Network in Ductile Hydroxyethylcellulose Matrix. *Soft Matter* **2011**, *7*, 7342−7350.
(40) Philipse, A. P.; Wierenga, A. M. On the Density and Structure Formation in Gels and Clusters of Colloidal Rods and Fibers. *Langmuir* **1998**, *14*, 49−54.
(41) Yamanaka, Y.; Esumi, K. Adsorption of Hydroxyethylcellulose or Hydrophobically Modified Cellulose and Anionic Surfactant from Their Binary Mixtures on Particles. *Colloids Surf., A* **1997**, *122*, 121−133.
(42) Zhao, G.; Chen, S. B. Clouding and Phase Behavior of Nonionic Surfactants in Hydrophobically Modified Hydroxyethyl Cellulose Solutions. *Langmuir* **2006**, *22*, 9129−9134.

(43) Paria, S.; Manohar, C.; Khilar, K. C. Adsorption of Anionic and Non-Ionic Surfactants on a Cellulosic Surface. *Colloids Surf., A* **2005**, *252*, 221−229.